THE JOURNAL OF PHYSICAL CHEMISTRY C

ARTICLE

pubs.acs.org/JPCC

Structural Analysis of Silica-Supported Molybdena Based on X-ray Spectroscopy: Quantum Theory and Experiment

C. S. Guo,[†] K. Hermann,[*,†] M. Hävecker,[‡,§] J. P. Thielemann,[§] P. Kube,[§] L. J. Gregoriades,[∥] A. Trunschke,[§] J. Sauer,[∥] and R. Schlögl[§]

[†]Theory Department, Fritz-Haber-Institut der Max-Planck-Gesellschaft, Faradayweg 4-6, 14195 Berlin, Germany

[‡]Department of Solar Energy Research, Helmholtz-Zentrum Berlin/BESSY II, Albert-Einstein-Str. 15, 12489 Berlin, Germany

[§]Inorganic Chemistry Department, Fritz-Haber-Institut der Max-Planck-Gesellschaft, Faradayweg 4-6, 14195 Berlin, Germany

[∥]Institut für Chemie, Humboldt-Universität zu Berlin, Unter den Linden 6, 10099 Berlin, Germany

ABSTRACT:

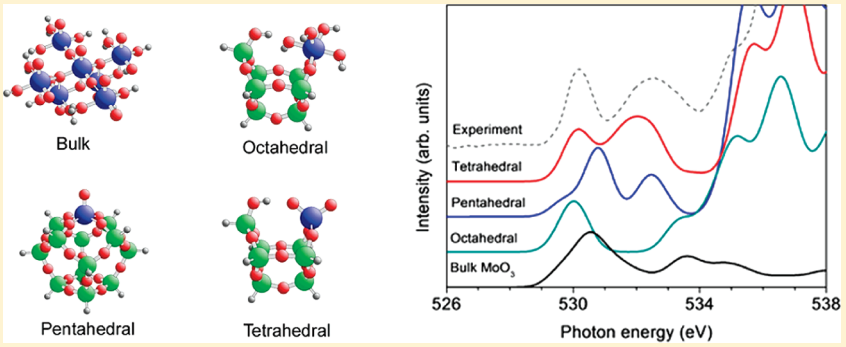

Oxygen core excitations in different molecular molybdena−silica models are evaluated using density-functional theory (DFT). These results can be compared with in situ X-ray absorption fine structure (NEXAFS) measurements near the O K-edge of molybdena model catalysts supported on SBA-15 silica, used for exploratory catalytic activity studies. The comparison allows an analysis of structural details of the molybdena species. The silica support is found to contribute to the NEXAFS spectrum in an energy range well above that of the molybdena units, allowing a clear separation between the corresponding contributions. Different types of oxygen species, O(1) in terminal M═O bonds, O(2) in interphase Mo—O—Si bridges and in Mo—O—Mo linkages, as well as O(2) in terminal Mo—O—H groups can be distinguished in the theoretical spectra of the molybdena species with molybdenum in tetrahedral (dioxo species), pentahedral (monooxo species), and octahedral coordination. The experimental NEXAFS spectra exhibit a pronounced double-peak structure in the O 1s to Mo 4d−O 2p excitation range of 529−536 eV. Comparison with the present theoretical data gives clear indications that dioxo molybdena species with tetrahedral MoO_4 units can explain the experimental spectrum. This does not fully exclude species with other Mo coordination, like pentahedral. However, the latter are believed to exist in the present samples in much smaller amounts. The experimental NEXAFS spectrum for the supported molybdena species differs substantially from that for MoO_3 bulk material with octahedral MoO_6 units where the observed asymmetric peak structure is also reproduced by the calculations.

1. INTRODUCTION

Molybdenum oxide is catalytically active in a wide range of different organic reactions, including oxidation, hydrogenation, metathesis, and isomerization, that require both redox and acid−base functions. Selective oxidation of propene to acrolein, oxidation of acrolein to acrylic acid, methanol oxidation, olefin metathesis, or hydroprocessing applications are prominent examples of commercially implemented molybdenum oxide based catalysts. Oxidation catalysts are often very complex, containing multiple active sites and different functionalities that may cooperate under operation conditions. Aiming at an improved fundamental understanding of oxidation catalysis, supported molybdenum oxide species have been studied as model catalysts in partial oxidation of different molecules, e.g., methanol,[1] propylene,[2] and propane.[3] Selectivity in partial oxidation is determined by the relative abundance of intermediates formed in the complex network of consecutive and parallel reactions. The actual reaction mechanism depends on the local geometric structure of surface metal oxide species and its interaction with the support, which determines the surface catalyst characteristics as a whole, including reducibility, acid base properties, and the nature of the active oxygen species. These parameters in turn are a function of the metal oxide loading, the chemistry of the support, and the preparation procedure. Therefore, detailed knowledge of the metal oxide surface structure is essential for the establishment of structure−function relationships, which are required for an improved con-

Received: April 13, 2011
Revised: June 24, 2011
Published: July 05, 2011

dx.doi.org/10.1021/jp2034642 | J. Phys. Chem. C 2011, 115, 15449–15458

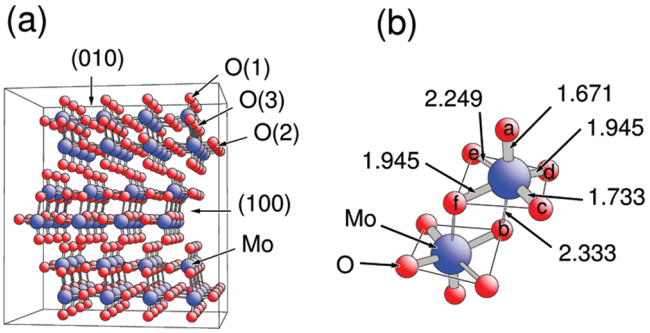

Figure 1. (a) Geometric structure of orthorhombic MoO_3 with bilayer stacking along the (010) direction. Molybdenum (oxygen) atoms are shown by large (small) balls. Nonequivalent oxygen atoms, O(1, 2, 3), are labeled accordingly. (b) Adjacent octahedral MoO_6 building units from the top and bottom part of the bilayers. The oxygen atoms are labeled a−f with interatomic Mo−O distances given in angstroms.

trol of selectivity in partial oxidation reactions. Extensive studies have been devoted to the investigation of relations between the electronic and geometric structure of surface vanadium oxide species and their reactivity in oxidative dehydrogenation and selective oxidation reactions.[3−8] These studies reveal analogies to supported molybdenum oxide catalysts which are generally less active than vanadia catalysts.[3] The origin of the different performance of the two catalysts is still unclear.

In this work, we perform density-functional theory (DFT) calculations on oxygen core excitations in molybdena−silica model clusters simulating local sections of supported molybdena catalysts as well as in clusters representing bulk MoO_3 substrate. The theoretical excitation spectra are then compared with in situ X-ray absorption fine structure (NEXAFS) measurements near the oxygen K-edge of molybdena model catalysts supported by SBA-15 silica in order to identify structural and electronic details of the molybdena species. NEXAFS spectroscopy[9] is based on dipole excitations of highly localized core electrons by photons. Thus, it can provide reliable atom-specific information allowing to distinguish between atoms in different local environments. This is used in the present calculations to discriminate between differently binding oxygen, in molybdenyl Mo═O as well as in Mo—O—Mo, Mo—O—Si, Mo—O—H, and Si—O—Si bridges of the silica-supported molybdena species. It also offers the possibility to identify specific molybdena species, such as tetrahedral MoO_4, pentahedral MoO_5, or octahedral MoO_6, among those prepared in this study experimentally at the surface of mesoporous silica, SBA-15.[10]

In section 2, we introduce the models and discuss details of the computational methods used in the spectrum calculations. Section 3 describes experimental details connected with sample preparation and NEXAFS measurements, while section 4 presents results and discussion. Finally, section 5 summarizes our conclusions.

2. THEORETICAL DETAILS

2.1. Cluster Models. The present calculations are based on molybdena−silica model clusters whose structures are obtained from chemical reasoning combined with structure optimizations at the DFT level in this study as well as from earlier work on the oxidation of methane[11] and methanol[12] on silica-supported molybdena. The clusters represent a variety of arrangements of molybdena in different coordinations where the MoO_x units are bound to silicon of the silica support via Mo−O−Si bridges.

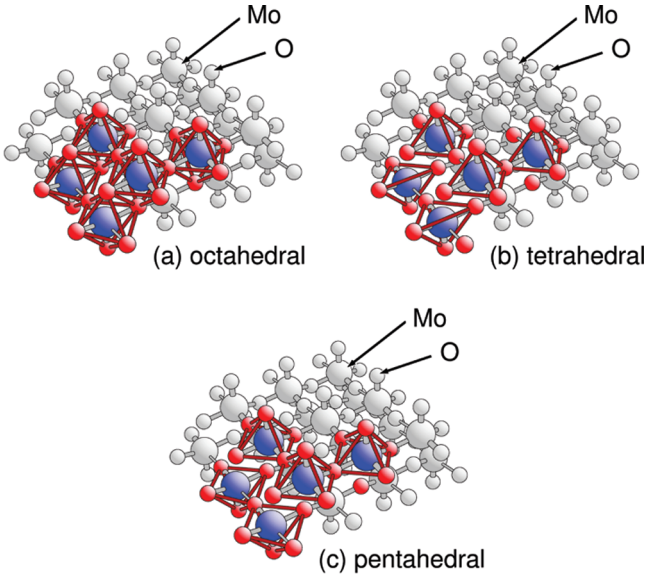

Figure 2. Geometric structure of MoO_3(010) bilayers illustrating the stacking of (a) octahedral MoO_6, (b) tetrahedral MoO_4, and (c) pentahedral MoO_5 building units; see the text. Molybdenum (oxygen) atoms are shown by large (small) balls.

Table 1. Molybdenum−Oxygen Bond Distances in the Model Clusters Simulating MoO_3 Bulk (Figure 3b) and Different Molybdena−Silica Clusters (Figure 4)[a]

cluster	$d_{Mo-O(1)}$	$d_{Mo-O(2)}$	$d_{Mo-O(3)}$
$Mo_7O_{30}H_{18}$ (bulk)	1.67	1.73 (2.25)	1.94 (1.94, 2.33)
cluster	d_1	d_2	d_3
(a) $MoO_3(OH)-Si_8O_{12}H_7$	1.72 (1.91)	1.90	
(b) $MoO_4-Si_7O_{10}H_8$	1.70	1.87	
(c) $(MoO_4)_2-Si_6O_7H_6$	1.70	1.89	
(d) $MoO(OH)_5-Si_8O_{12}H_7$	1.88−1.97	2.02	
(e) $MoO_2(OH)_4-Si_7O_{10}H_8$	1.89−1.96	1.93, 1.96	
(f) $MoO_4(OH)_2-Si_{12}O_{16}H_{12}$	1.92	1.92−1.93	
(g) $MoO_5-Si_4O_4H_4$	1.68	1.94	
(h) $MoO_5-Si_{12}O_{16}H_{12}$	1.68	1.91	
(i) $Mo_2O_8-Si_6O_7H_6$	1.68	1.89	1.85 (2.08)

[a] For the MoO_3 bulk cluster, $Mo_7O_{30}H_{18}$, distances $d_{Mo-O(1)}$, $d_{Mo-O(2)}$, and $d_{Mo-O(3)}$ denote those of terminal molybdenyl, Mo═O, of asymmetric Mo—O—Mo bridges, and of symmetric Mo—O—Mo bridges with an additional longer Mo—O distance. For the molybdena−silica clusters, distances d_1 refer to those of terminal molybdenyl Mo═O (or Mo—OH for clusters a, d, e, and f), d_2 to those of Mo—O—Si bridges, and d_3 to those of Mo—O—Mo bridges. All distances are in angstroms; see also Figure 1b.

These arrangements were inspired to some extent by the geometric structure of bulk MoO_3 which forms an orthorhombic crystal lattice with a layer structure of weakly binding bilayers parallel to (010) netplanes; see Figure 1a. Each bilayer consists of two interleaved sheets which can be described by distorted MoO_6 octahedra sharing corners while octahedra from adjacent planes share edges;[13,14] see Figure 2a. The asymmetry of the octahedra, with four smaller Mo−O distances (1.67−1.94 Å) and two larger d_{Mo-O} values (2.25−2.33 Å),[13] see Table 1 and Figure 1b,

dx.doi.org/10.1021/jp2034642 |J. Phys. Chem. C 2011, 115, 15449–15458

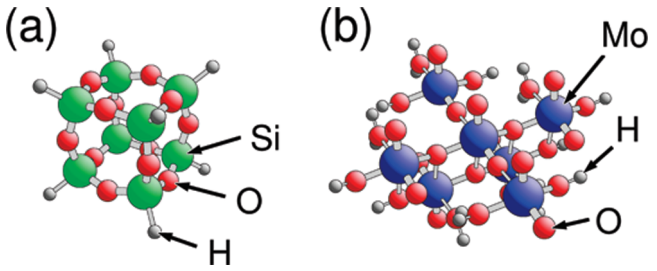

Figure 3. Geometric structure of the model clusters representing (a) the silica support (silsesquioxane, $Si_8O_{12}H_8$) and (b) the MoO_3 bulk substrate ($Mo_7O_{30}H_{18}$); see the text. Atoms are shown by balls of different radii and labeled accordingly.

suggests an alternative characterization of each bilayer by two parallel sheets which are composed of ribbons of MoO_4 tetrahedra sharing corners along the (001) direction; see Figure 2b. A third possible molybdenum coordination may be derived by considering the bilayers of bulk MoO_3 to consist of two parallel sheets each forming networks of corner linked pyramidal MoO_5 units with their tops pointing in opposite directions; see Figure 2c. These three equivalent descriptions result in octahedral, tetrahedral, and pentahedral oxygen environments around molybdenum which may be taken as separate molybdena units of corresponding coordination.

The silica support of the molybdena−silica clusters is modeled by clusters[15] which are derived from polyhedral oligomeric silsesquioxane (POSS), $Si_8O_{12}H_8$.[16] This molecule is of cubic structure with silicon occupying the corners and oxygen near the edge midpoints while hydrogen saturates the dangling bonds at the silicon corners; see Figure 3a. A molybdena species is added to this molecule or to corresponding fragments to yield the molybdena−silica model clusters shown in Figure 4. Here, Figures 4a−c represent clusters in which monomeric and dimeric dioxo molybdena species appear with the molybdenum atoms in 4-fold tetrahedral coordination, (a) $MoO_3(OH)-Si_8O_{12}H_7$ with molybdena bound by one Mo−O−Si bridge with the silica support, (b) $MoO_4-Si_7O_{10}H_8$ with two Mo−O−Si bridges, and (c) $(MoO_4)_2-Si_6O_7H_6$, yielding two adjacent dioxo molybdena binding as in (b) each.

Figures 4d−f show clusters containing octahedrally coordinated monomeric molybdena species, (d) $MoO(OH)_5-Si_8O_{12}H_7$ with one Mo−O−Si bridge, (e) $MoO_2(OH)_4-Si_7O_{10}H_8$, and (f) $MoO_4(OH)_2-Si_{12}O_{16}H_{12}$ with four Mo−O−Si bridges. Figures 4g−i refer to clusters describing pentahedrally coordinated monooxo molybdena, (g) $MoO_5-Si_4O_4H_4$ and (h) $MoO_5-Si_{12}O_{16}H_{12}$ with four Mo−O−Si bridges and (i) $Mo_2O_8-Si_6O_7H_6$, yielding two adjacent monooxo molybdena binding with two Mo−O−Si and Mo−O−Mo bridges each. Note that models d and e are obtained by H_2O addition near the Mo centers of models a and b, respectively, and cluster f arises from H_2O addition to model h. As this is an endothermic process with increasing Gibbs free energy, models d, e, and f represent less stable structures than models a, b, and h, respectively.

Reference calculations on molybdena environments in bulk MoO_3 are based on a $Mo_7O_{30}H_{18}$ cluster, see Figure 3b, describing a local section of a bilayer parallel to (010) netplanes shown in Figure 1. Here, dangling Mo−O bonds at the cluster periphery are saturated by hydrogen to account for cluster embedding. Corresponding Mo−O distances of all clusters are listed in Table 1; see also Figure 1b.

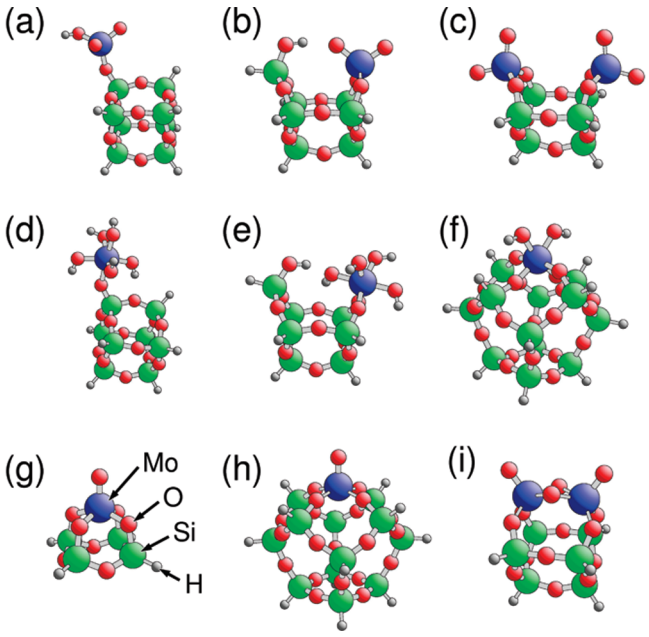

Figure 4. Geometric structure of the molybdena−silica model clusters: (a−c) Tetrahedrally coordinated dioxo molybdena species. (d−f) Octahedrally coordinated molybdena species. (g−i) Pentahedrally coordinated monooxo molybdena species; see the text. Atoms are shown by balls of different radii and labeled accordingly in part g.

2.2. NEXAFS Spectrum Calculations. Electronic ground and core excited states of the above clusters are calculated within density-functional theory (DFT) using the gradient corrected revised Perdew−Burke−Ernzerhof (RPBE) exchange-correlation functional.[17,18] Corresponding Kohn−Sham orbitals are represented by linear combinations of atomic orbitals (LCAO) using extended basis sets of contracted Gaussians. For the evaluation of X-ray absorption spectra, silicon and hydrogen are represented by all-electron double-ζ-valence-plus-polarization (DZVP) basis sets while the electronic structure of molybdenum is described by an effective core potential (ECP) together with a valence basis set for the 14 outermost valence electrons. At the core excited oxygen center, extended IGLO-III type basis sets[19] are employed to adequately describe inner shell relaxation effects while the other oxygen centers in the cluster are accounted for by effective core potentials (ECPs) for the 1s shell and corresponding valence basis sets.[20,21] For all calculations, the DFT cluster code StoBe[22] is employed.

The computation of theoretical O 1s X-ray absorption spectra of the different clusters considers core to unoccupied orbital excitations resulting from dipole transitions. Thus, polarization-resolved spectral intensities $I(E, \mathbf{e})$ are determined by corresponding dipole transition matrix elements, vectors $\mathbf{m} = (m_x, m_y, m_z)$, together with angle-dependent factors describing the polarization vector $\mathbf{e} = (e_x, e_y, e_z)$ of the incoming radiation, i.e., by

$$I(E, \mathbf{e}) = \alpha \cdot E \cdot (\mathbf{me})^2, \quad \mathbf{m} = \langle \varphi_f | q \cdot \mathbf{r} | \varphi_{core} \rangle \qquad (1)$$

Here, α is a global scaling factor, E denotes the transition energy, and transition dipole vectors $\mathbf{m}$ involve the initial core orbital φ_{core} and final excited state orbitals φ_f. For the present purpose, the complex dependence of the spectral intensities on the photon polarization direction can be ignored due to the disordered arrangement of the MoO_x particles to be considered. Therefore, the

angle averaged intensity given by

$$I(E) = \int I(E, \mathbf{e})\, d\Omega = 2\pi/3 \cdot \alpha \cdot E \cdot (m_x^2 + m_y^2 + m_z^2) \quad (2)$$

and summed over all possible final state orbitals φ_f will be used in the analysis. The evaluation of core excited final states and corresponding matrix elements $\mathbf{m}$ is performed within the transition potential approach[23] in combination with a double basis set technique.[24] This approximation involves the use of a half occupied O 1s core orbital at the ionization site, thereby accounting for partial electronic relaxation due to the presence of the excited electron. It has been proven earlier that, within this approach, final state relaxation effects are taken care of up to second order in the energy, achieving a balance between the two relaxation mechanisms, core and valence type.[25]

The computed orbital energies and corresponding dipole transition matrix elements in eq 2 are convoluted using Gaussian broadening of varying width to simulate instrumental, vibrational, and lifetime broadening. A full-width-at-half-maximum (fwhm) value of 1 eV is applied below the ionization threshold while the broadening is increased linearly to 4 eV up to 20 eV above threshold and kept fixed at this value for higher energies. In the transition potential approach, the electronic core hole relaxation of the excited final state is not fully accounted for. This incomplete relaxation can be corrected in an approximate way by shifting all excitation energies by the difference of the ionization potential computed with the transition potential method and the corresponding value from ΔKohn−Sham (ΔSCF) calculations. This results in a global downward shift of about 2 eV. Further, relativistic corrections are included by applying an additional upward shift of the computed spectra by 0.33 eV.[26]

The present computational approach has been used successfully to yield highly accurate results for X-ray absorption of light atoms in gas phase molecules.[27−29] It has also been used to study properties of hydrogen-bonded systems,[27,30,31] of adsorbates on metal surfaces,[32,33] and of differently coordinated oxygen sites near vanadium and molybdenum oxide surfaces.[34−36] Further details concerning the methods can be found in the corresponding references.

3. EXPERIMENTAL DETAILS

3.1. Synthesis of the Silica-Supported Molybdena and Oxidative Dehydrogenation of Propane. The synthesis of MoO_x/SiO_2 was adapted from a functionalization/anion exchange procedure applied previously in the preparation of silica supported vanadia catalysts.[37,38] The mesoporous support, which was synthesized based on the original recipe of Yang et al.,[39] was functionalized using 3-aminopropyltrimethoxysilane (APTMS) followed by protonation of the resulting amine with HCl. The chloride ions were exchanged by heptamolybdate ions applying ammonium heptamolybdate ($(NH_4)_6Mo_7O_{24}\cdot 4H_2O$) as the Mo precursor. The resulting powder was washed, filtered, and calcined at 823 K for 12 h. The samples included in the present study contained a molybdenum loading of 5.9 and 11.1 wt %. A SBA-15 reference sample was prepared applying the same procedure as described above. However, potassium oxalate monohydrate was introduced in the material instead of heptamolybdate in the ion-exchange step.

The SBA-15 supported molybdenum oxide catalyst containing 11.1 wt % molybdenum (internal catalyst ID 6870) was tested in the oxidative dehydrogenation of propane for temperatures between 723 and 773 K applying contact times between 0.05 and 0.6 gs/ml and a molar ratio of propane/oxygen = 2:1 with nitrogen as balance ($C_3H_8/O_2/N_2$ = 10/5/85). The experiments were carried out in a setup for selective oxidation (Integrated Lab Solutions, Berlin, Germany) using eight parallel fixed bed quartz reactors at atmospheric pressure. For the measurements, 100 mg of the catalyst was diluted with 2.9 g of silicon carbide (ratio 1:30) for minimization of temperature gradients. Reactants and products were analyzed by an online gas chromatograph (Agilent 7890). Separation of the permanent gases CO, CO_2, N_2, and O_2 was achieved with a combination of a Plot-Q and a Plot-molsieve column connected to a thermal conductivity detector (TCD). Propane and propylene were separated with a Plot-Q column connected to a flame ionization detector (FID).

3.2. NEXAFS Measurements. In situ NEXAFS measurements have been performed at the synchrotron radiation facility BESSY II of the Helmholtz-Zentrum Berlin, Germany (HZB), using monochromatic radiation of the ISISS (Innovative Station for In Situ Spectroscopy) beamline as a tunable X-ray source. High pressure soft X-ray absorption spectra were measured in the presence of oxygen at elevated temperature using the high pressure station designed and constructed at the Fritz-Haber Institute, Berlin. Details of the setup are described elsewhere.[40−42] In brief, self-supporting pellets of MoO_x/SBA-15 samples are mounted inside a reaction cell onto a sapphire sample holder approximately 1.4 mm in front of the first aperture of a differentially pumped electrostatic lens system. The home-built electron lens serves as the input system for a modified commercial hemispherical electron analyzer (PHOIBOS 150, Specs-GmbH). Oxygen is introduced into the cell via calibrated mass flow controllers, heating is provided by a NIR laser at the rear of the sample, and the temperature is monitored by a thermocouple attached directly to the sample surface. NEXAFS spectra of the dehydrated MO_x/SBA-15 samples have been obtained in 0.5 mbar O_2 at 350 °C by heating the material in situ in the XAS cell at 5 K/min up to the final temperature. Oxygen 1s (K-edge) excitation spectra have been recorded in the Auger electron yield mode by operating the electron spectrometer with a pass energy of 100 eV as an XAS detector to minimize contributions from the gas phase to the spectra. O K-edge spectra of the sample surface have been corrected for the remaining effects of O_2 gas phase absorption. In order to increase the signal-to-noise ratio, a data reduction by a factor of 6 has been applied to the raw spectra (containing about 4000 pts per scan) by averaging adjacent points. Three scans have been averaged, and the X-ray spot position on the sample has been changed after each scan to avoid damage of the surface by the brilliant synchrotron X-ray beam. Absolute energy calibration has been achieved by setting the π^* resonance of the O_2 gas phase signal to 530.9 eV, and the spectral resolution was about 150 meV. Further details of the metrology and data treatment are presented elsewhere.[43] The polycrystalline reference bulk sample of α-MoO_3 has been prepared by suspending commercial powder (Fluka) in chloroform on a steel plate to create a thin film of material without charging.

4. RESULTS AND DISCUSSION

Due to the well-defined preparation procedure, the present silica supported molybdenum oxide catalyst seems adequately

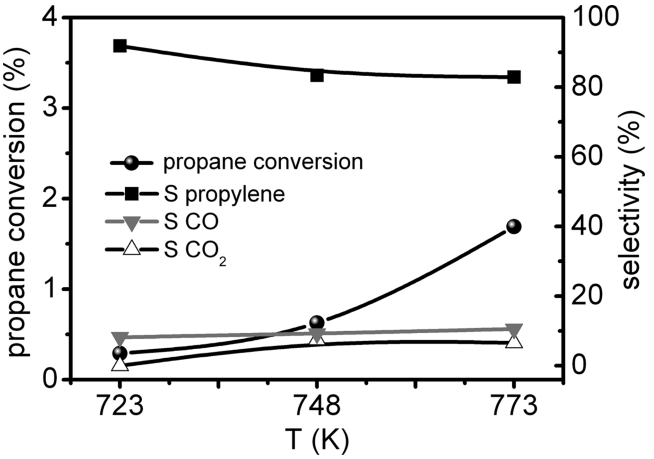

Figure 5. Propane conversion and product selectivity in oxidative dehydrogenation of propane over 11.1%Mo/SBA-15 for a contact time of 0.6 gs/ml in a feed mixture containing the reactants in a molar ratio of $C_3H_8/O_2/N_2 = 10/5/85$.

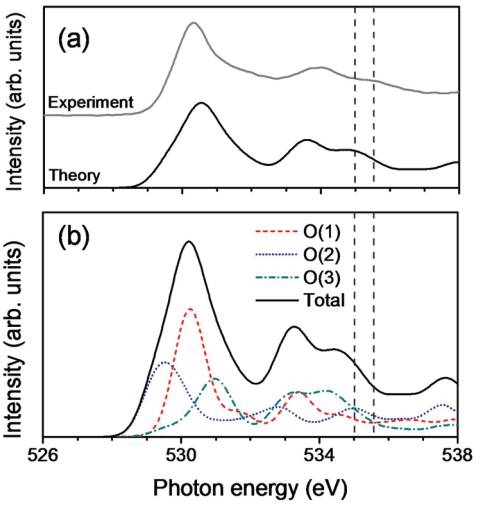

Figure 6. (a) Comparison of the theoretical oxygen 1s core excitation spectrum ("Theory") evaluated for the model cluster $Mo_7O_{30}H_{18}$ (Figure 2b) with an experimental O K-edge NEXAFS spectrum for bulk MoO_3 ("Experiment"). (b) Decomposition of the theoretical excitation spectrum into contributions from the three differently coordinated oxygen sites, O(1), O(2), O(3), see Figure 1a. The two vertical dashed lines indicate the energy range of the computed ionization potentials of the three differently coordinated oxygen species.

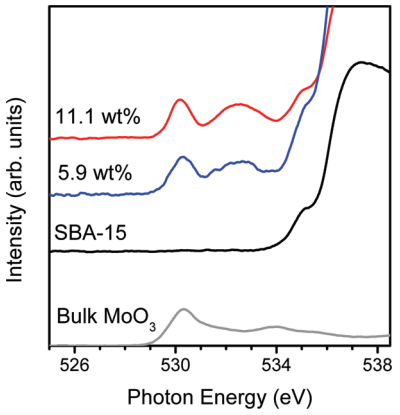

Figure 7. Experimental O K-edge NEXAFS spectra for dehydrated MoO_x/SBA-15 with 5.9 and 11.1 wt % Mo loading; see the text. The NEXAFS spectra for clean SBA-15 substrate and bulk MoO_3 are included for comparison.

suited as a model to gain new insight into the nature of the active sites as well as into relations between structural properties and activity with emphasis on oxidation reactions. The SBA-15 supported molybdenum oxide catalyst containing 11.1 wt % molybdenum is found to be active in oxidative dehydrogenation of propane. Its activity was studied in a temperature range between 723 and 773 K (Figure 5). For a contact time of 0.6 gs/ml, propane conversion reaches a maximum of approximately 2%. Under these conditions, only small amounts of total and partial oxidation products CO_2 and CO are formed, resulting in a propylene selectivity of more than 80%. The Arrhenius plot using the propane consumption rate yields an apparent activation energy of 162 kJ/mol. This is considerably high compared to values reported in the literature for molybdenum oxide species supported on other carrier oxides. The apparent activation energy of propane activation has been determined to be 117 kJ/mol on $11\%MO_x/ZrO_2$ (ref 5) and 97 kJ/mol on $5\%MoO_x/TiO_2$ (ref 4) for catalysts with molybdenum oxide loadings corresponding to a theoretical monolayer. This substantiates the strong effect of the support in oxidative dehydrogenation of propane.

4.1. NEXAFS Spectra for Bulk MoO_3. Before examining the silica-supported MoO_x particles, we validate our theoretical methods for bulk MoO_3 whose structure is well-known.[13,14] For this compound, experimental oxygen K-shell NEXAFS spectra are available in the literature[36] but have also been re-examined in this study. Figure 6a compares the calculated oxygen 1s core excitation spectrum for a model cluster $Mo_7O_{30}H_{18}$ with H termination at its periphery, see Figure 3b, representing a crystal section of α-MoO_3 bulk (considered earlier in theoretical studies[13]) with corresponding experimental O K-edge NEXAFS data for samples of clean α-MoO_3 bulk. Both spectra reveal a main peak near 530.5 eV and a broader double peak structure between 533.5 and 535 eV where the comparison suggests very good agreement considering the fact that an absolute energy scale without adjustment between theory and experiment is used. This gives confidence that the present theoretical methods can also give a reliable description of the spectroscopic data for small supported MoO_x particles.

The theoretical bulk spectrum of Figure 6a can be characterized in detail by analyses of corresponding final state orbitals. The peak structure between 530 and 535 eV is found to be dominated by O 1s core excitations to unoccupied orbitals with antibonding O 2p−Mo 4d character. Further, the broad peak at lower energy refers to final state orbitals where the O 2p admixture points perpendicular to the corresponding O−Mo bond, whereas the peaks at higher energy are due to orbitals with O 2p admixture pointing along the O−Mo bond. Thus, the different amount of antibonding character of the two types of orbitals explains the energetic peak sequence. Figure 6b shows a decomposition of the total theoretical bulk spectrum into individual contributions from the three nonequivalent bulk oxygen species, O(1), O(2), O(3), as defined in Figure 1a. Obviously, the broad low energy peak in the total spectrum originates from three individual peaks shifted by about 1 eV with respect to each other and referr-

dx.doi.org/10.1021/jp2034642 |J. Phys. Chem. C 2011, 115, 15449–15458

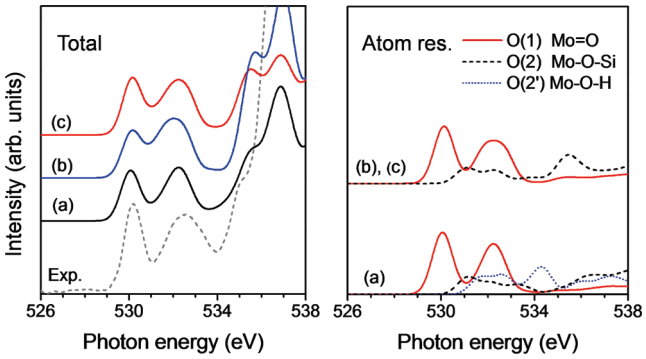

Figure 8. (left, Total) Theoretical O 1s core excitation spectra for clusters a−c containing tetrahedral MoO_4 subunits; see Figure 4. The spectra are compared with experimental O K-edge NEXAFS data (dashed line) for dehydrated Mo_xO_y/SBA-15 with 11.1 wt % Mo taken from Figure 7. (right, Atom res.) Decomposition of the excitation spectra into contributions from different oxygen species in clusters a−c, terminal molybdenyl oxygen O(1), O(2) in Mo−O−Si bridges, and O(2′) in Mo−O−H bridges. The atom resolved spectra of clusters b and c are almost identical.

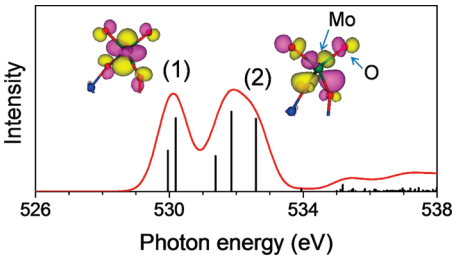

Figure 9. Theoretical O 1s excitation spectrum calculated for molybdenyl oxygen O(1) in the MoO_4−$Si_7O_{10}H_8$ cluster (b); see Figure 4b. The figure includes discrete excitation energies of the two-peak region shown as vertical lines of lengths determined by the excitation probabilities. The iso-surface plots illustrate representative final state orbitals 1 and 2 near the centers of the two peaks; see the text.

ing to different oxygen species where the central peak is slightly larger in intensity than the other two and due to molybdenyl O(1) excitations. The peak structure at higher energies in the total spectrum is a somewhat more complex superposition of individual peaks where also excitations from all oxygen species contribute.

4.2. Experimental NEXAFS Spectra for SBA-15 Silica and Supported MoO_x Particles. Figure 7 compares experimental oxygen K-edge NEXAFS spectra of the SBA-15 silica support with those of adsorbed MoO_x particles of two different molybdenum loadings, 11.1 and 5.9 wt %, at the SBA-15 surface. In addition, the bottom spectrum shows the NEXAFS result for crystalline MoO_3 bulk measured with the same experimental setup. The spectrum for the clean SBA-15 support reveals one large asymmetric peak near 538 eV with a smaller precursor at 535 eV. The origin of these peaks has been analyzed earlier in theoretical cluster studies[44] and found to be due to oxygen 1s core excitations of Si−O−Si bridges in the SBA-15 support. Deposition of dehydrated molybdena at the support yields for both loadings two additional peaks, one low energy peak of 0.9 eV fwhm at 530.2 eV and a broader peak structure of 1.9 eV fwhm at 532.5 eV where the integral intensities of the two peaks are rather similar. These peaks must originate from core excitations of oxygen located at the MoO_x particles. It is interesting to compare the NEXAFS spectra for deposited molybdena with that of crystalline MoO_3 bulk also included in Figure 7 and discussed in the previous section. Obviously, the two types of samples show rather different spectral behavior in the oxygen K-edge region. This suggests a different geometric arrangement of the oxygen in deposited molybdena compared with that inside the MoO_3 bulk in which distorted octahedral MoO_6 units exist. On the other hand, the two-peak structure found in the NEXAFS spectra for deposited molybdena has been shown to resemble that observed for crystalline sodium molybdate, $Na_2MoO_4 \cdot 2H_2O$,[45] containing tetrahedral MoO_4 units only.[46] This may indicate structural similarity with corresponding MoO_x units at the SBA-15 support.

4.3. Theoretical NEXAFS Spectra for MoO_x−SiO_2 Model Clusters. *4.3.1. Model Clusters with Tetrahedral MoO_4 Units.* Figure 8 shows theoretical O 1s core excitation spectra for the three molybdena−silica model clusters in which the molybdenum of the molybdena subunits is tetrahedrally coordinated (dioxo MoO_4 species), as shown in Figure 4a−c. The left diagram ("Total") collects total spectra composed of stoichiometrically weighted superpositions of partial spectra due to excitation at the different types of oxygen, terminal molybdenyl, as well as 2-fold bridging. Obviously, the three clusters yield a two-peak structure in the excitation energy range between 529 and 534 eV with a slightly narrower peak centered near 530.3 eV and a broader peak near 532.0 eV. The integral intensity of the higher energy peak is only slightly larger than that of the lower energy peak. Both the peak positions and their intensities are found to be extremely similar for the three clusters. This suggests that the actual geometric coupling of the dioxo MoO_4 species with the silica support, by one Mo−O−Si bridge in cluster a of Figure 4 and by two Mo−O−Si bridges in clusters b and c, influences the spectral features very little. In addition, the close similarity between the spectra for clusters b and c, in which one and two (adjacent) MoO_4 species exist, indicates that the O 1s core excitations are highly local processes which are affected only little by the electronic interaction with nearby MoO_4 species.

The right diagram of Figure 8 ("Atom res.") shows a decomposition of the excitation spectra into contributions from different oxygen species in clusters a−c, terminal oxygen O(1) of molybdenyl Mo═O, O(2) in interphase Mo—O—Si bridges, and O(2′) in Mo—O—H bridges (cluster a only). Contributions from oxygen O(2#) in Si—O—Si bridges of the silica support appear only above 535 eV and are not included in the figure. A comparison of the atom resolved spectra with the corresponding total excitation spectra evidence that for all three clusters the two-peak structure in the energy region between 529 and 534 eV is determined mainly by core excitations at the molybdenyl oxygen O(1) while contributions from the bridging oxygen species appear at higher energies. The broad peak at 536.5 eV appearing in cluster a and attributed to core excitations in Mo—O—Si bridges is shifted to lower energies, 535.6 eV, and reduced in its width for clusters b and c. This is simply due to the different electronic coupling of the tetrahedrally coordinated MoO_4 species which binds with one Mo—O—Si bridge to the silica substrate in cluster a but with two bridges in clusters b and c.

The type of oxygen core excitations of the double-peak spectrum in the energy region between 529 and 534 eV can be characterized in greater detail by examining corresponding final state orbitals. As an example, Figure 9 shows the partial spectrum obtained for 1s core excitation at molybdenyl oxygen O(1) in the MoO_4−$Si_7O_{10}H_8$ cluster (b); see Figure 4b. The figure includes

dx.doi.org/10.1021/jp2034642 |J. Phys. Chem. C 2011, 115, 15449–15458

also discrete excitation energies of the double-peak region given by vertical lines of lengths determined by the excitation probabilities. This shows that the energetically lower peak at 530.3 eV in the spectrum originates from two excitations separated by 0.3 eV where the excitation at lower energy contributes about 60% in intensity compared with that at higher energy (main excitation). Further, the energetically higher peak near 532 eV combines three excitations separated by 0.5 and 0.8 eV, respectively, where the lowest excitation yields about 50% intensity compared with each of the two higher excitations which are roughly equal in intensity. The final state orbitals referring to these core excitations can be analyzed in detail by their atom contributions or by populations. All orbitals of the double-peak structure are found to represent antibonding mixtures of major Mo 4d and smaller O 2p contributions, the latter at the excitation center O(1). The amount of antibonding character determines the energetic order of the excitations. The orbital type is also obvious in corresponding three-dimensional iso-surface plots. As an illustration, Figure 9 shows plots of two final state orbitals resulting from (1) the main excitation of the energetically lower peak and (2) the topmost excitation of the higher peak. These orbitals are focused mainly at the MoO_4 unit of the model cluster with only very little orbital admixture from remote oxygen and silicon centers. (Only the MoO_4 part of the cluster is shown in Figure 9.) An inspection of the orbital shapes evidences the 4d type orbital character near the molybdenum center of the MoO_4 unit for both final state orbitals. Further, the orbital contributions at the oxygen center (excitation center, labeled "O" in the right plot) are clearly of 2p type in both cases. In addition, the antibonding character of the Mo−O coupling is obvious from the iso-surfaces in the region between the two atom centers which differ in color (shading) for positive and negative orbital values. Obviously, the directions of the O 2p functions at the excitation centers differ. For final state orbital 1 of the low energy peak, the p function points perpendicular to the Mo−O(1) bond axis, yielding less antibonding character than found for orbital 2 of the high energy peak where the p function points almost along the Mo−O(1) bond axis.

Figure 8 includes also the experimental O K-edge NEXAFS data (dashed line) for dehydrated Mo_xO_y/SBA-15 with 11.1 wt % Mo taken from Figure 7. This spectrum shows, in the energy region between 529 and 534 eV, a striking similarity with the theoretical excitation spectra of all three molybdena−silica model clusters containing tetrahedrally coordinated dioxo MoO_4 species. The agreement refers to both the energetic positions of the two-peak structure (the energy scale has not been adjusted between theory and experiment) and the relative intensities of the peaks. This may suggest that the dehydrated MoO_x prepared in the SBA-15 support can be characterized structurally as tetrahedrally coordinated dioxo MoO_4 species. However, for a conclusive structural confirmation, other molybdena types need to be considered as will be discussed in the following.

4.3.2. Model Clusters with Octahedral MoO_6 Units. Figure 10 shows theoretical O 1s core excitation spectra for the three molybdena−silica model clusters with octahedrally coordinated molybdena subunits (MoO_6 species), as shown in Figure 4d−f. The left diagram ("Total") gives total spectra resulting from stoichiometrically weighted superpositions of partial spectra due to excitation at the different types of 2-fold coordinated bridging oxygen. The total spectra of the three clusters yield, in the excitation energy range between 529 and 534 eV, a main peak at 529.8 eV and a much smaller peak at 3.0−3.5 eV above the main peak. The peak positions and their relative intensities turn out to

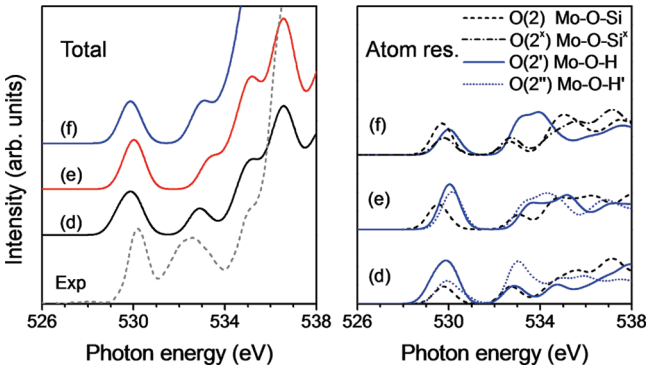

Figure 10. (left, Total) Theoretical O 1s core excitation spectra for clusters d−f containing octahedral MoO_6 subunits; see Figure 4. The spectra are compared with experimental O K-edge NEXAFS data (dashed line) for dehydrated Mo_xO_y/SBA-15 with 11.1 wt % Mo taken from Figure 7. (right, Atom res.) Decomposition of the excitation spectra into contributions from different oxygen species in clusters d−f, $O(2^{(x)})$ in Mo−O−Si bridges, and $O(2')$ and $O(2'')$ in different representative Mo−O−H bridges.

be rather similar for the three clusters. This indicates, analogous to the tetrahedral MoO_4 species discussed in section 4.3.1, that the actual geometric coupling of the MoO_6 species with the silica support, by one, two, or four Mo−O−Si bridges in clusters d, e, and f, respectively, affects the spectral features rather little.

The right diagram of Figure 10 ("Atom res.") shows a decomposition of the excitation spectra into contributions from different oxygen species in clusters d−f, O(2) and $O(2^x)$ of the two types of Mo−O−Si bridges as well as $O(2')$ and $O(2'')$ of the two types of Mo−O−H bridges. Contributions from oxygen $O(2^{\#})$ in Si−O−Si bridges of the silica support appear only above 535 eV and are not included in the figure. They explain, however, the third peak near 535 eV in the total spectra of the three clusters. A comparison of the atom resolved spectra with the corresponding total excitation spectra shows that for all three clusters the main peak at 529.8 eV is characterized as a mixture of contributions due to oxygen core excitations both in Mo−O−Si and Mo−O−H bridges. Here, the relative intensities of Mo−O−Si compared with Mo−O−H bridges increase in going from cluster d to e which can be understood as a simple stoichiometric effect. As a result of the different coupling of the MoO_6 species with the silica support, the ratio of Mo−O−Si to Mo−O−H bridges is 1:5 for cluster d and 2:4 and 4:2 for clusters e and f, respectively. The smaller peak near 533 eV in the total spectrum is explained by the atom decomposition as mainly due to oxygen core excitations in Mo−O−H bridges characterizing the dangling OH groups of the hydrolyzed MoO_6 species.

The types of oxygen core excitations appearing in the total spectra in the energy region between 529 and 534 eV have been examined by analyzing corresponding final state orbitals. Overall, the qualitative results agree with those obtained for the tetrahedral MoO_4 species discussed in section 4.3.1. All final state orbitals can be described as antibonding mixtures of major Mo 4d and smaller O 2p contributions where the amount of antibonding character determines the energetic order of the excitations.

Figure 10 includes also the experimental O K-edge NEXAFS data (dashed line) for dehydrated Mo_xO_y/SBA-15 with 11.1 wt % Mo taken from Figure 7. This spectrum with its almost symmetric double-peak structure between 529 and 534 eV looks rather different compared with the theoretical excitation spectra

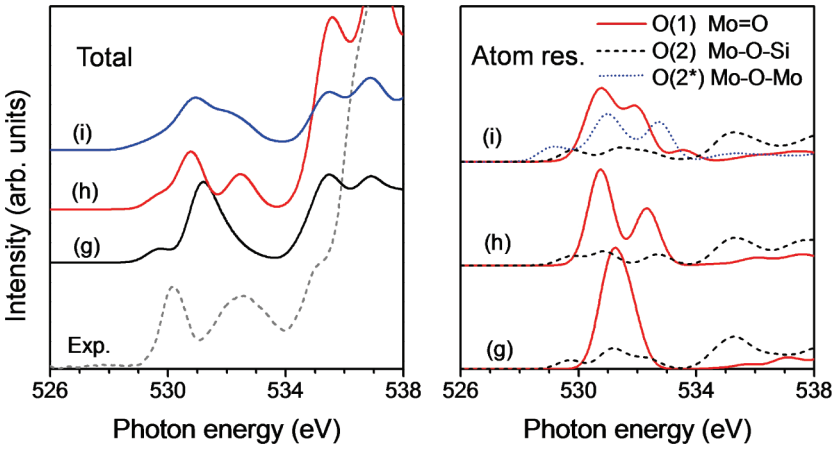

Figure 11. (left, Total) Theoretical O 1s core excitation spectra for clusters g—i containing pentahedral MoO_4 subunits; see Figure 4. The spectra are compared with experimental O K-edge NEXAFS data (dashed line) for dehydrated Mo_xO_y/SBA-15 with 11.1 wt % Mo taken from Figure 7. (right, Atom res.) Decomposition of the excitation spectra into contributions from different oxygen species in clusters g—i, terminal molybdenyl oxygen O(1) and O(2) in Mo—O—Si bridges, and O(2*) in Mo—O—Mo bridges.

of the three molybdena—silica model clusters containing octahedrally coordinated MoO_6 species. This applies to both the relative intensities of the two peaks found in the theoretical spectra and their energetic separation which is too large in all cases. The disagreement suggests that the dehydrated catalytically active MoO_x prepared on the SBA-15 support may not reflect octahedrally coordinated MoO_6 species. The discrepancy is consistent with the unfavorable relative Gibbs free energy of the octahedral compared with the tetrahedral species mentioned earlier.

4.3.3. Model Clusters with Pentahedral MoO_5 Units. Figure 11 shows theoretical O 1s core excitation spectra for the three molybdena—silica model clusters in which the molybdenum of the molybdena subunits is pentahedrally coordinated (monoxo MoO_5 species), as shown in Figure 4g—i. The left diagram ("Total") gives total spectra resulting from stoichiometrically weighted superpositions of partial spectra due to excitation at the different types of oxygen, terminal molybdenyl, and 2-fold bridging. The right diagram ("Atom res.") shows a decomposition of the excitation spectra into contributions from different oxygen species in clusters g—i, terminal oxygen O(1) of molybdenyl Mo═O, O(2) of mixed Mo—O—Si bridges, and O(2*) of Mo—O—Mo bridges (cluster i only).

Obviously, the total spectra are quite different between the three model clusters which can be explained by the rather different structure of the MoO_5 units and their coupling with the silica support in the clusters. In the smallest model, cluster g, the molybdena unit is anchored at a four-membered silicate ring. This constrains the four Mo—O—Si bridges to an angle $\Theta_{Mo-O-Si}$ = 119.5° which reflects an unusually strong Mo—O—Si tilt. (Interestingly, cluster g has been used in theoretical studies of catalytic methane[11,47] oxidation.) Here, the total spectrum is described by a large main peak at 531.3 eV which, from the atom decomposition of the spectrum, is characterized by core excitations of molybdenyl oxygen O(1). The very small side peak at lower energy is identified as being due to core excitations of oxygen in Mo—O—Si bridges. These excitations contribute also smaller intensity to the main peak as well as to a minor peak near 535 eV which overlaps energetically with the region of core excitations of oxygen in Si—O—Si bridges of the silica support.

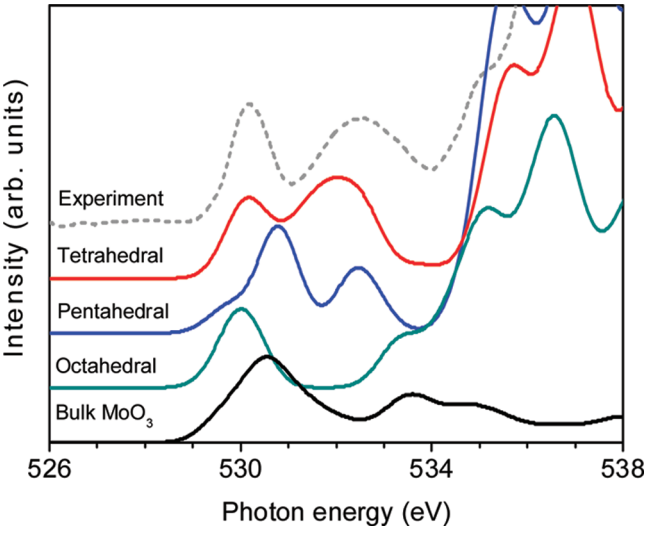

Figure 12. Comparison of theoretical O 1s core excitation spectra for MoO_x/SiO_2 clusters reflecting tetrahedral (cluster b of Figure 4), pentahedral (cluster h), and octahedral (cluster e) molybdenum coordination. The figure includes for comparison the corresponding theoretical spectrum for MoO_3 bulk (cluster b of Figure 3) as well as experimental O K-edge NEXAFS data (dashed line) for dehydrated Mo_xO_y/SBA-15 with 11.1 wt % Mo; see Figure 7.

In model cluster h, the molybdena—silica binding is also achieved by four Mo—O—Si bridges. However, these involve Si sites of an eight-membered silicate ring which allows a much less pronounced tilt of the Mo—O—Si bridges, given by an angle $\Theta_{Mo-O-Si}$ = 160.6°. This seems more reasonable compared with the tilt in cluster g. (The superiority of model h over model g has also been pointed out earlier in theoretical reaction studies.[12]) The total spectrum of O 1s core excitations of cluster h is composed of two main peaks, one at 530.9 eV with an additional low energy shoulder at 529.7 eV and one of smaller intensity at 532.5 eV. The atom decomposition shows that both peaks are due to core excitations of molybdenyl oxygen, while the low energy shoulder is attributed to excitations of oxygen in Mo—O—Si bridges. Analogous to the results for cluster g, oxygen excitations in Mo—O—Si bridges

dx.doi.org/10.1021/jp2034642 |J. Phys. Chem. C 2011, 115, 15449–15458

lead also to a peak near 535 eV which overlaps with the energy region of core excitations of oxygen in Si−O−Si bridges.

Model cluster i contains two MoO_5 units which couple with each other via two Mo−O−Mo bridges and bind with the silica support by two Mo−O−Si bridges. This binding scheme is different from those of the previous two clusters g and h and affects the total spectrum of O core excitations greatly. The spectrum is described by a broad peak structure in the energy range between 529 and 534 eV. Here, the peak maximum lies at 531 eV with a smaller shoulder at 532.3 eV and a broadening asymmetry near 529 eV. A comparison with the atom resolved spectra, see right diagram of Figure 11, shows that the peak structure is dominated by core excitations of both molybdenyl oxygen and oxygen in Mo−O−Mo bridges where the latter cover a somewhat wider energy range. However, the integral contributions given by the peak areas are about equal for the two oxygen species. Core excitations at oxygen in Mo−O−Si bridges lead also to a peak near 535 eV, as discussed for the previous clusters.

The experimental O K-edge NEXAFS data for dehydrated Mo_xO_y/SBA-15 with 11.1 wt % Mo (dashed line in Figure 11, taken from Figure 7) was shown to yield an almost symmetric double-peak structure between 529 and 534 eV. A comparison with the theoretical excitation spectra of the molybdena−silica model clusters containing pentahedrally coordinated MoO_5 species evidence disagreement in the peak structures for all three cases. Cluster h, for which the comparison shows the smallest disagreement, yields an additional low-energy shoulder which is not observed. Further, the energetic separation between the two main peaks is too small by 1 eV compared with experiment. Finally, the peak intensity ratio is quite different from experiment. Altogether, the agreement of the calculated spectra for the pentahedrally coordinated monooxo MoO_5 species with those measured for MoO_x on SBA-15 support is much less convincing than for the tetrahedrally coordinated dioxo MoO_4 species.

5. CONCLUSIONS

In this study, we have evaluated theoretical oxygen 1s core excitation spectra of silica-supported molybdena model clusters and of clusters for MoO_3 bulk using DFT cluster techniques. The results are then compared with spectra of in situ O K-edge NEXAFS measurements for polycrystalline MoO_3 bulk as well as for dehydrated molybdena of different concentration on SBA-15 support. Here, MoO_x/SBA-15 has been shown to be catalytically active in the oxidative dehydrogenation of propane to propylene; see Figure 5. The experiments are typical for a catalyst precursor in the presence of oxygen and in the absence of any coordinating ligand, such as water, fixing the highest oxidation state of Mo.

In the calculations, the partial core excitation spectra of differently binding oxygen species, molybdenyl Mo═O, as well as oxygen in Mo—O—Mo, Mo—O—Si, Mo—O—H, and Si—O—Si bridges of the silica-supported molybdena species, are found to differ considerably as to their peak shapes and energy distributions. Therefore, their spectral superposition in different molybdena units, tetrahedral dioxo MoO_4, octahedral MoO_6, and pentahedral monooxo MoO_5, distinguish between the units in stoichiometrically well-defined material. This can be used to explain spectral details of in situ NEXAFS measurements on the SBA-15 supported molybdena model catalysts and, thus, to draw conclusions about a possible existence of different molybdena species.

Experimental O K-edge NEXAFS data for samples of clean α-MoO_3 bulk exhibit a large main peak near 530.5 eV and a broader less intense double peak structure between 533.5 and 535 eV; see Figure 6a. This spectrum is quite nicely reproduced by that of the present cluster model calculations. On the other hand, O K-edge NEXAFS spectra of dehydrated molybdena on SBA-15 support yield, for energies between 529 and 534 eV, a clear double-peak structure with a low energy peak at 530.2 eV and a broader peak at 532.5 eV where the integral intensities of the two peaks are rather similar, as shown in Figure 7. These spectra are obviously quite different from those obtained for MoO_3 bulk, hinting at different local geometric MoO_x structure. The present theoretical analysis of oxygen 1s core excitation spectra for different molybdena units in various molybdena−silica clusters can give a rather clear assignment. First, spectral contributions from core excited oxygen in Si—O—Si bridges of the silica support are found to appear only above 535 eV, i.e., energetically well separated from the observed double-peak structure. Second, the energy range between 529 and 534 eV is clearly attributed to oxygen core excitations where those in molybdenyl Mo═O groups or Mo—O—Si, Mo—O—H, and Mo—O—Mo bridges contribute. Further, molybdenyl excitations are found to dominate the spectral shape in most cases.

Among the computed spectra for supported tetrahedral MoO_4, octahedral MoO_6, and pentahedral MoO_5, shown in Figures 8, 10, and 11, those for the tetrahedrally coordinated dioxo MoO_4 species yield the best agreement with experiment. Those for the pentahedral monooxo species agree less well (cluster h yields an additional low-energy shoulder which is not observed, and the energetic separation between the two main peaks is too small by 1 eV compared with experiment). Finally, octahedral MoO_6 species cannot explain the measured spectrum at all. This is emphasized in Figure 12 comparing theoretical O 1s core excitation spectra for the differently coordinated molybdena where, for each coordination, the computed cluster spectrum fitting best with experiment was chosen. It suggests strongly that the dehydrated molybdena prepared in the SBA-15 support of the present study does not contain octahedrally coordinated MoO_6 units. It is assumed to contain tetrahedrally coordinated dioxo MoO_4 as the dominant species, while a pentahedrally coordinated monooxo species seems to exist in only small quantities if at all. For other catalyst preparations, the relative composition of the different molybdena species may vary from the present result. As an example, we mention Raman and infrared measurements on MoO_x/SiO_2 samples[48] where computational studies[12] suggest the coexistence of tetra- and pentahedrally coordinated molybdena species. Theoretical and experimental studies of other molybdena reference compounds, such as molybdates whose structures are well-known, may help to get deeper insight into the structure of supported molybdena catalysts. They may serve as a foundation for in situ reaction studies where the separation of active phase signatures from those of the support as well as the local coordination of the Mo species is important. Studies along these lines are currently under way.

AUTHOR INFORMATION

Corresponding Author

*E-mail: hermann@fhi-berlin.mpg.de.

ACKNOWLEDGMENT

This work was partly supported by the Deutsche Forschungsgemeinschaft (DFG) through its Collaborative Research Centre 546, “Transition metal oxide aggregates”. The HZB staff is

acknowledged for continuously supporting the synchrotron based high pressure electron spectroscopy experiments of the Fritz-Haber Institute at BESSY II. Furthermore, the authors thank Prof. Christian Hess, Tech. Univ. Darmstadt, for fruitful discussions.

REFERENCES

(1) Jehng, J.-M.; Hu, H.; Gao, X.; Wachs, I. E. *Catal. Today* **1996**, *28*, 335.
(2) Desikan, A. N.; Zhang, W. M.; Oyama, S. T. *J. Catal.* **1995**, *157*, 740.
(3) Chen, K.; Bell, A. T.; Iglesia, E. *J. Phys. Chem. B* **2000**, *104*, 1292.
(4) Heracleous, E.; Machli, M.; Lemonidou, A.; Vasalos, I. A. *J. Mol. Catal. A: Chem.* **2005**, *232*, 29.
(5) Khodakov, A.; Olthof, B.; Bell, A. T.; Iglesia, E. *J. Catal.* **1999**, *181*, 205.
(6) Wachs, I. E.; Weckhuysen, B. M. *Appl. Catal., A* **1997**, *157*, 67.
(7) Hess, C. *ChemPhysChem* **2009**, *10*, 319.
(8) Muylaert, I.; Voort, P. V. D. *Phys. Chem. Chem. Phys.* **2009**, *11*, 2826.
(9) Stöhr, J. *NEXAFS spectroscopy*; Springer: Berlin, New York, 1992.
(10) Ying, J. Y.; Mehnert, C. P.; Wong, M. S. *Angew. Chem., Int. Ed.* **1999**, *38*, 56.
(11) Chempath, S.; Bell, A. T. *J. Catal.* **2007**, *247*, 119.
(12) Gregoriades, L. J.; Döbler, J.; Sauer, J. *J. Phys. Chem. C* **2010**, *114*, 2967.
(13) Hermann, K.; Witko, M. In *Oxide Surfaces*; Woodruff, D. P., Ed.; The Chemical Physics of Solid Surfaces, Vol. 9; Elsevier: Amsterdam, The Netherlands, 2001; p 136.
(14) Kihlborg, L. *Ark. Kemi* **1963**, *21*, 357, 443, 461. *Acta Chem. Scand.* **1963**, *17*, 1485.
(15) Sauer, J.; Hill, J.-R. *Chem. Phys. Lett.* **1994**, *218*, 333.
(16) Feher, F. J.; Walzer, J. F. *Inorg. Chem.* **1991**, *30*, 1689.
(17) Hammer, B.; Hansen, L. B.; Nørskov, J. K. *Phys. Rev. B* **1999**, *59*, 7413.
(18) Perdew, J. P.; Burke, K.; Ernzerhof, M. *Phys. Rev. Lett.* **1996**, *77*, 3865.
(19) Kutzelnigg, W.; Fleischer, U.; Schindler, M. *NMR Basic Principles and Progress*; Springer: Berlin, New York, 1990.
(20) Nyberg, M. Ph.D. Thesis, Stockholm University, 2000.
(21) Pettersson, L. G. M.; Wahlgren, U.; Gropen, O. *J. Chem. Phys.* **1987**, *86*, 2176.
(22) Hermann, K.; Pettersson, L. G. M. deMon developers group, StoBe software V. 3.1, 2011; see http://www.fhi-berlin.mpg.de/KHsoftware/StoBe/.
(23) Triguero, L.; Pettersson, L. G. M.; Ågren, H. *Phys. Rev. B* **1998**, *58*, 8097.
(24) Ågren, H.; Carravetta, V; Vahtras, O; Pettersson, L. G. M. *Chem. Phys. Lett.* **1994**, *222*, 75.
(25) Leetmaa, M.; Ljungberg, M. P.; Lyubartsev, A.; Nilsson, A.; Pettersson, L. G. M. *J. Electron Spectrosc. Relat. Phenom.* **2010**, *177*, 135.
(26) Takahashi, O.; Pettersson, L. G. M. *J. Chem. Phys.* **2004**, *121*, 10339.
(27) Cavalleri, M.; Odelius, M.; Nordlund, D.; Nilsson, A.; Pettersson, L. G. M. *Phys. Chem. Chem. Phys.* **2005**, *7*, 2854.
(28) Kolczewski, C.; Püttner, R.; Martins, M.; Schlachter, A. S.; Snell, G.; Sant'Anna, M.; Hermann, K.; Kaindl, G. *J. Chem. Phys.* **2006**, *124*, 034302.
(29) Kolczewski, C.; Püttner, R.; Plashkevych, O.; Ågren, H.; Staemmler, V.; Martins, M.; Snell, G.; Schlachter, A. S.; Sant'Anna, M.; Kaindl, G.; Pettersson, L. G. M. *J. Chem. Phys.* **2001**, *115*, 6426.
(30) Cavalleri, M.; Näslund, L.Å.; Edwards, D. C.; Wernet, P.; Ogasawara, H.; Myneni, S.; Öjamäe, L.; Odelius, M.; Nilsson, A.; Pettersson, L. G. M. *J. Chem. Phys.* **2006**, *124*, 194508.
(31) Wernet, P.; Nordlund, D.; Bergmann, U.; Cavalleri, M.; Odelius, M.; Ogasawara, H.; Näslund, L.Å.; Hirsch, T. K.; Ojamae, L.; Glatzel, P.; Pettersson, L. G. M.; Nilsson, A. *Science* **2004**, *304*, 995.
(32) Öström, H.; Ogasawara, H.; Näslund, L. Å.; Pettersson, L. G. M.; Nilsson, A. *Phys. Rev. Lett.* **2006**, *96*, 146104.
(33) Schiros, T.; Haq, S.; Ogasawara, H.; Takahashi, O.; Öström, H.; Andersson, K.; Pettersson, L. G. M.; Hodgson, A.; Nilsson, A. *Chem. Phys. Lett.* **2006**, *429*, 415.
(34) Kolczewski, C.; Hermann, K. *Surf. Sci.* **2004**, *552*, 98.
(35) Kolczewski, C.; Hermann, K. *J. Chem. Phys.* **2003**, *118*, 7599.
(36) Cavalleri, M.; Hermann, K.; Guimond, S.; Romanyshyn, Y.; Kuhlenbeck, H.; Freund, H. J. *Catal. Today* **2007**, *124*, 21.
(37) Hess, C.; Hoefelmeyer, J. D.; Tilley, T. D. *J. Phys. Chem. B* **2004**, *108*, 9703.
(38) Hess, C.; Wild, U.; Schlögl, R. *Microporous Mesoporous Mater.* **2006**, *95*, 339.
(39) Yang, P.; Zhao, D.; Margolese, D. I.; Chmelka, B. F.; Stucky, G. D. *Nature* **1998**, *396*, 152.
(40) Vass, E. M.; Hävecker, M.; Zafeiratos, S.; Teschner, D.; Knop-Gericke, A.; Schlögl, R. *J. Phys.: Condens. Matter* **2008**, *20*, 1.
(41) Bluhm, H.; Hävecker, M.; Knop-Gericke, A.; Kiskinova, M.; Schlögl, Salmeron, R. M. *MRS Bull.* **2007**, *7*, 602.
(42) Knop-Gericke, A.; Kleimenov, E.; Hävecker, M.; Blume, R.; Teschner, D.; Zafeiratos, S.; Schlögl, R.; Bukhtiyarov, V. I.; Kaichev, V. V.; Prosvirin, I. P.; Nizovskii, A. I.; Bluhm, H.; Barinov, A.; Dudin, P.; Kiskinova, M. *Adv. Catal.* **2008**, *52*, 215.
(43) Hävecker, M.; Cavalleri, M.; Herbert, R.; Follath, R.; Knop-Gericke, A.; Hess, C.; Hermann, K.; Schlögl, R. *Phys. Status Solidi B* **2009**, *246*, 1459.
(44) Cavalleri, M.; Hermann, K.; Knop-Gericke, A.; Hävecker, M.; Herbert, R.; Hess, C.; Oestereich, A.; Döbler, J.; Schlögl, R. *J. Catal.* **2009**, *262*, 215.
(45) Thielemann, J. P. PhD thesis, Tech. Univ., Darmstadt, 2011.
(46) Bramnik, K. G.; Ehrenberg, H. *Z. Anorg. Allg. Chem.* **2004**, *630*, 1336.
(47) Chempath, S.; Zhang, Y.; Bell, A. T. *J. Phys. Chem. C* **2007**, *111*, 1291.
(48) Lee, E. L.; Wachs, I. E. *J. Phys. Chem. C* **2007**, *111*, 14410.